



FLUCOME 2009

10th International Conference on Fluid Control, Measurements, and Visualization
August 17–21, 2009, Moscow, Russia

COMPUTATIONAL STUDY OF SEPARATION CONTROL MECHANISM WITH THE IMAGINARY BODY FORCE ADDED TO THE FLOWS OVER AN AIRFOIL

Kengo Asada¹ and Kozo Fujii²

ABSTRACT

The effects of body force distribution on the control of airfoil separation flow are discussed. Steady body force is applied to the separation flow around the NACA0012 airfoil near the leading edge, and two-dimensional Favre-averaged Navier-Stokes equations are solved by conventional CFD method. In this paper, six body force models are considered. Mach number is 0.1 and Reynolds number based on the chord length is 100,000. The following characteristics are observed from the present results. The model applying the body force near the airfoil surface can restrain the airfoil flow separation than the model applying body force far from the airfoil surface. Therefore, body force near the airfoil surface is effective on the separation control. However, in the direction along the airfoil surface, the width of the region at which the body force acts is not very effective to the separation control. Finally, the body force in the vertical direction to the airfoil surface does not so much affect the separation control.

Keywords: Airfoil, Body force, CFD, Flow control, Separation flow

INTRODUCTION

Separation control of the flow over airfoils has been studied, and vortex generator and jet flap are conventionally used for separation flow control. However, these conventional devices have some faults such as complexity and heavy, or becoming a drag on the cruising. On the other hand, recently micro active flow control devices have attracted attention. For example, DBD (Dielectric Barrier Discharge) plasma actuator (Post and Corke, 2004; Font and Morgan 2005; Roth and Dai, 2006; Tsubakino and Fujii, 2007; Asada *et al.*, 2009) and synthetic jet (Seifert *et al.*, 1996) can change the operating conditions according to surroundings. In addition, these device systems are relatively simple and have light weight. Fig. 1 shows a DBD plasma actuator installed at the wing leading edge. DBD plasma actuator can be installed by only putting it on the airfoil surface, and it has a very simple constitution which is composed of two dielectrics and a electrode. These advantages are very useful for MAV (Micro Air Vehicle) or Mars

¹ Corresponding author: Department of Aeronautics and Astronautics, University of Tokyo, 3-1-1, Yoshinodai, Sagamihara, Kanagawa, 229-8510, Japan, e-mail: asada@flab.isas.jaxa.jp

² JAXA Institute of Space and Astronautical Science, 3-1-1, Yoshinodai, Sagamihara, Kanagawa, 229-8510, Japan, e-mail: fujii@flab.isas.jaxa.jp

airplane (Guynn et al., 2003), which is paid attention in recent years. Because small size airplane such as a MAV is weak at the sudden disturbance like a gust, active flow control capability is useful for it. In addition, the size and weight of Mars airplane are limited by mission requirement, and the Martian atmosphere has a stronger gust than the earth. Therefore, Mars airplane needs the device which is small and has the active control capability. That is why recently, active flow control devices which is simple and light weight have been studied very well.

However, most of previous studies are focused on respective devices such as a pulsed jet, a synthetic jet and a DBD plasma actuator. There is little common knowledge about active flow control between these devices, though it seems that every device applies some disturbances to the flow. Moreover, these respective devices research is hard to extract the important parameter because these devices are limited in operating conditions on each device. On synthetic jet, nondimensional frequency relate to Reynolds number. So, it is difficult to separate the each parameter effect. Therefore, the objective of the present study is to organize what type of disturbance is effective on the airfoil flow separation control and clarify the mechanism how to control the separation by substituting body force for the disturbance using numerical calculation. As the first step of the present study, steady body force is applied to the airfoil flow near the leading edge, and the effects of body force distribution on the control of airfoil separation flow are discussed.



Fig. 1. DBD plasma actuator installed at the wing leading edge

COMPUTATIONAL MODELS

Governing equations

Two-dimensional Favre-averaged Navier-Stokes equations are employed as the governing equations in this study. They consist of the mass, the momentum and the energy conservation laws. In the nondimensional form, governing equations are represented as follows:

$$\frac{\partial \rho}{\partial t} + \frac{\partial \rho u_k}{\partial x_k} = 0 \quad (1)$$

$$\frac{\partial \rho u_i}{\partial t} + \frac{\partial (\rho u_i u_k + p \delta_{ik})}{\partial x_k} = \frac{1}{Re} \frac{\partial \tau_{ik}}{\partial x_k} + D_c F_i \quad (2)$$

$$\begin{aligned} \frac{\partial e}{\partial t} + \frac{\partial ((e+p)u_k)}{\partial x_k} &= \frac{1}{Re} \frac{\partial u_l \tau_{kl}}{\partial x_k} \\ &+ \frac{1}{(\gamma-1)PrReM_\infty^2} \frac{\partial q_k}{\partial x_k} + D_c u_k F_k \end{aligned} \quad (3)$$

Where u_i , q_i , ρ_i , p , e , τ_{ij} , δ_{ij} and t are the velocity vector, heat flux vector, density, static pressure, total energy per unit value, stress tensor, Kronecker's delta and time respectively. Three basic nondimensional numbers Re , Pr and M_∞ denote the Reynolds number, the Prandtl number and the free stream Mach number respectively:

$$Re = \frac{\rho_\infty u_\infty L_{chord}}{\mu_\infty}, \quad M_\infty = \frac{u_\infty}{a_\infty}, \quad Pr = \frac{\mu_\infty c_p}{k_\infty} \quad (4)$$

Where μ , L_{chord} , a , c_p and k are the viscosity, chord length of the wing, speed of sound, specific heat at constant pressure and heat conduction coefficient and the subscript “ ∞ ” represents free stream quantities. In Eq. (2), (3), the end term of right-hand side represents the body force and the energy added to unit volume respectively by active flow control device. These details are referred in next subsection.

It is well-known that the separation phenomenon is unsteady phenomenon. Only LES (Large-Eddy Simulation) or DNS (Direct Numerical Simulation) approach can resolve the unsteady flow structure. Furthermore, previous study have shown that LES/ RANS (Reynolds-Averaged Navier-Stokes) hybrid method can simulate such phenomenon well (Kawai and Fujii, 2005). However, our objective of this paper is not to clarify the turbulence structure, but to clarify fundamental effect of the body force distribution on separation control. The RANS simulations can give us the enough qualitative data of time-averaged flow fields. For this reason, the RANS simulation is employed. Baldwin and Lomax turbulence model (Baldwin and Lomax, 1978) is used for the RANS computation and fully turbulence field is assumed. Though this assumption cannot enable the simulations to capture the turbulence transition, enough data of the qualitative effect of the plasma actuator on separated flows are obtained.

Imaginary body force models

In previous subsection, it is mentioned that active flow control device is modeled as $D_c F_i$ and $D_c u_k F_k$ in Navier-Stokes equations. This modeling method refers to plasma actuator modeling. D_c is the nondimensional number relating electromagnetic force and determines the magnitude of body force. F_i represent the distribution of body force. F_i is determined referring Suzen model (Suzen and Huang, 2006), and six body force models including Suzen model are considered.

Suzen model is known as the model which can induce the practical velocity in flow by configuring the D_c value (Tsubakino and Fujii, 2007). In this paper, D_c is configured as $D_c = 8$ in order to induce the velocity in the same range as free stream velocity. The body force distribution image of Suzen model is shown in Fig. 2 and Fig. 3 (a). In these figures, the contour shows the body force magnitude, and the yellow vectors show the body force direction. In Fig. 2, the upper region is the flow region, and the lower region is the rigid body region. This figure shows that the Suzen model has two remarkable body forces. One of these forces is the force along the airfoil surface, and another force is the force perpendicular to the rigid body.

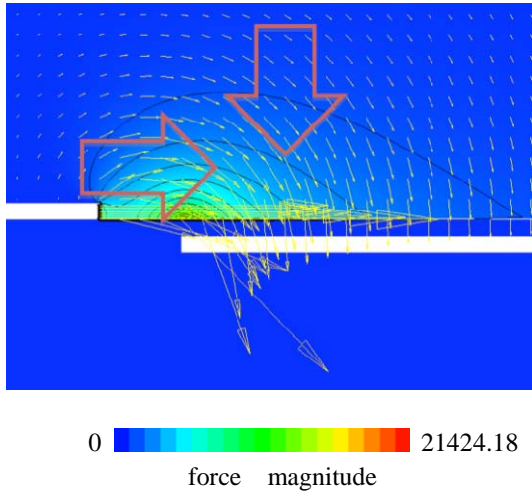


Fig. 2. Force distribution of Suzen model (DC=8)

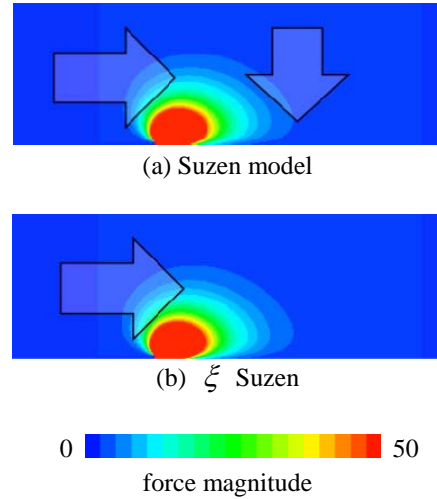


Fig. 3. Force distribution of Suzen model and ξ Suzen model (Dc=8).

In this paper, the six body force models referring Suzen model are discussed. One of the models is the Suzen model, which is a numerical calculation model for DBD plasma actuator. Another model is the Suzen model without the force in vertical direction to the airfoil surface (Fig. 3). Other four models are showed in Fig. 4. These models are based on the Suzen model but simpler spatial distribution, and considered to compare the effect of the distribution of body force in the vertical direction to the airfoil surface on separation control. Each model imposes the same amount of momentum in the direction along the airfoil surface to the flow. The region at which these models add the body force is 0.015 chord length for the airfoil surface direction, and 0.005 chord length for the vertical direction to the airfoil surface. The body force distribution of case 1 is homogeneously-distributed. Case 2 is the model applying body force far from the airfoil surface. Case 3 is the model applying the body force near the airfoil surface. And case 4 is also the model applying the body force near the airfoil surface but has shorter body force region in the direction along the airfoil surface.

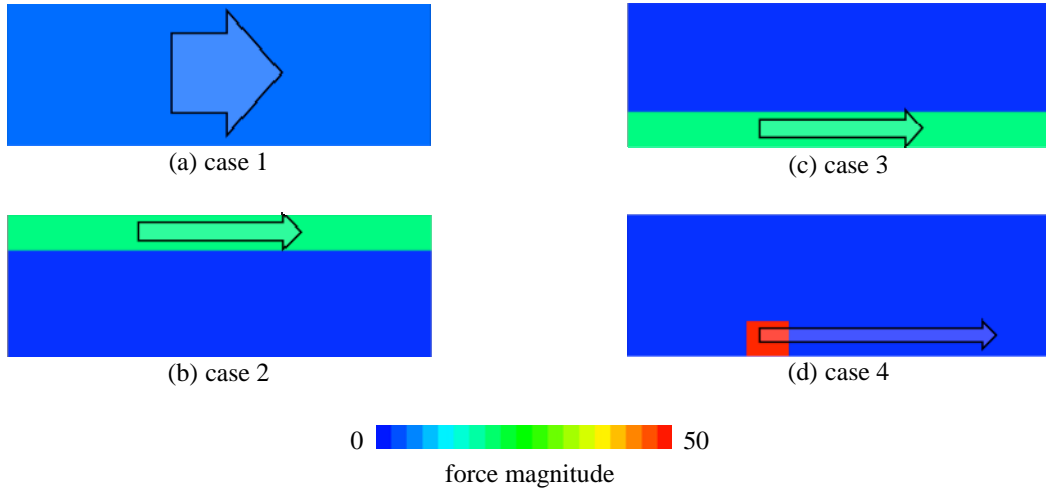


Fig. 4. Body force distribution of 4 models (Dc=8)

COMPUTATIONAL SETUP

Flow conditions

Free-stream Mach number is $M_\infty = 0.1$. When DBD plasma actuator is assumed as a active flow control device, in present technology, the velocity which DBD plasma actuator can induce several meters per second and the chosen free-stream Mach number seems to be high. However, the value is low enough that the compressibility of fluid is almost negligible. Therefore, the flow field obtained by our simulation is considered to be similar to that with a lower free-stream velocity. The Mars airplane is targeted, and other flow conditions are based on the Mars atmosphere. Reynolds number based on the chord length is considered is relatively low $Re_c = 100,000$. The specific heat ratio is set to be $\gamma = 1.34$. However, γ hardly effect on the flow field because M_∞ is low. The Prandtl number is set to 0.72. All discussions use the time-averaged flow field in this study.

Computational method

The Simple High-resolution Upwind Scheme (SHUS) (Shima and Jounouchi, 1997), which is belongs to the Advection Upstream Splitting Method (AUSM) (Liou and Steffen, 1991) type schemes, is applied to discretization of the convection terms. With using the physical values evaluated by the Monotone Upwind Scheme for Conservation Law (MUSCL) (Van Leer, 1977) approach based on the primitive variables, the SHUS scheme can keep third-order accuracy. The viscous terms are evaluated by the second-order central difference. For time integration, the ADI-SGS implicit method is used. This algorithm is extended one of Four-Factored Symmetric Gauss-Seidel (FF-SGS) (Fujii, 1999), which adopts both ideas of the Lower-Upper Symmetric Alternating Direction Implicit (LU-ADI) (Fujii and Obayashi, 1986) and the Lower-Upper Symmetric Gauss-Seidel (LU-SGS) (Yoon and Jameson, 1988).

Computational grids

The zonal method is employed to treat the body force small region. The grids consist of two parts, the airfoil grid and the region corresponding to the body force model region. Fig. 5 shows the computational grids, and in this figure, body force model is located at 0.005 chord length from the leading edge. Computation procedure is following three steps. At first, set the body force distribution on the body force model grid. Then, interpolate the body force to the Zone 2 grid. Finally, solve Eq. (1), (2) and (3) in Zone 1 and Zone 2 and interpolate physical values each other. Zone 1 is the C type grid and the length from the wing surface to the exterior boundary is 20 times chord length. These grid resolutions are follows; the body force model region has approximately 960,000, the Zone 2 has approximately 16,000 points, and the Zone 1 has approximately 120,000 points.

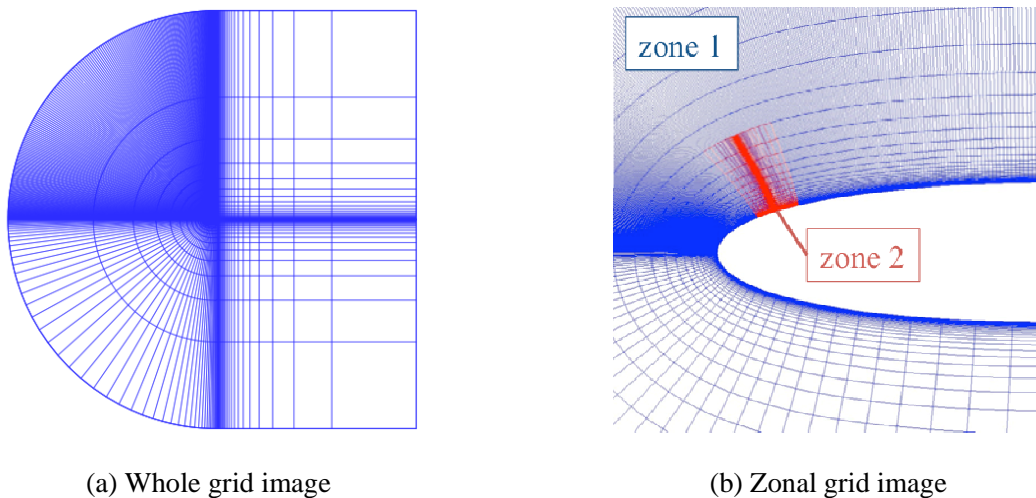


Fig. 5. Computational zonal grids

RESULTS AND DISCUSSIONS

Lift curves for each model (case 1 ~ case 2) and the no controlled case (off) are shown in Fig. 6. In this figure, No control case stalled at 16 deg, and when the peak of negative pressure of the lift coefficient distribution is smaller than -6 at 16 deg or more, the angle of attack defined as the massive flow separation point. Lift curves are plotted until the massive flow separation point. This figure show that each body force model improve the aerodynamic characteristics, and this is corresponding to the previous study (Tsubakino and Fujii, 2007). The case 2 has stalled at $\alpha=18$ deg, and the case 1 has stalled at $\alpha=19$ deg.

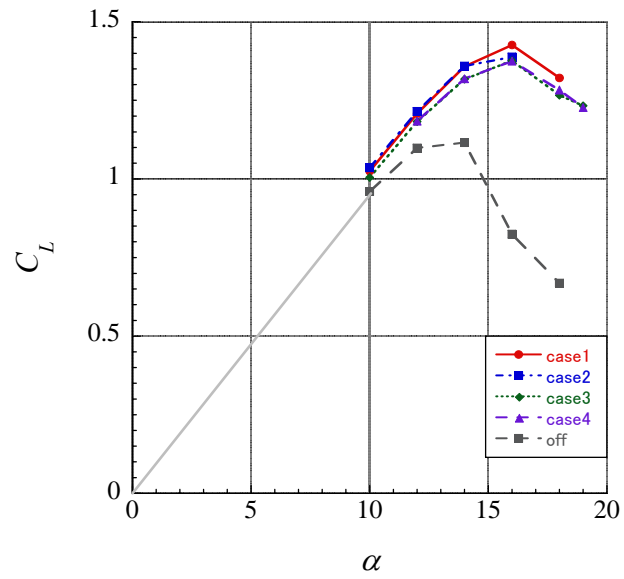
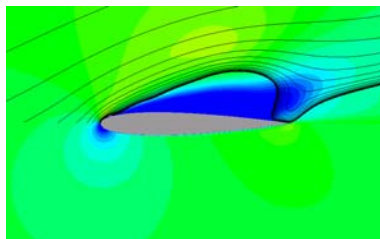
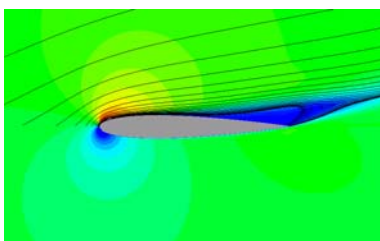


Fig. 6. Lift curves for each model



(a) case 2



(b) case 3

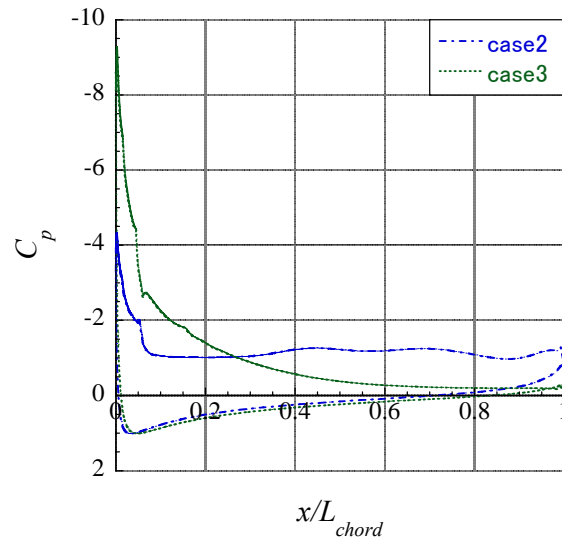
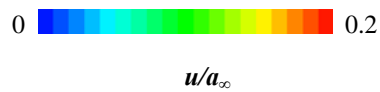
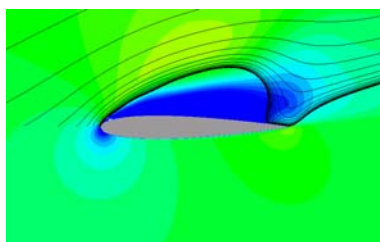


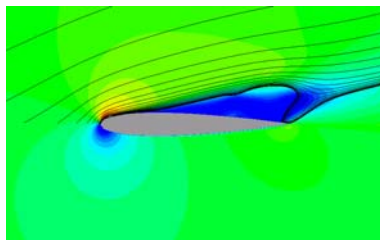
Fig. 7. Flow-fields with stream lines on the case 2 and the case 3 at $\alpha = 18$ deg

Fig. 8. C_p distributions on at case 2 and the case 3 at $\alpha = 18$ deg

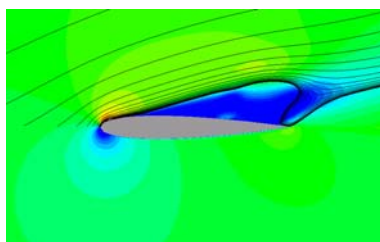
Next, respective case (case 1 ~ case 2) flow-fields are compared. In Fig. 7, the flow fields with stream lines are shown at $\alpha=18$ deg. The contour surface shows the horizontal direction velocity. This figure show that the case 2 has the massive flow separation from the leading edge, but the separation region is only near the trailing edge, on the case 3. In Fig. 8, C_p distributions on case 2 and the case 3 at $\alpha=18$ deg is shown. The case 2 has the C_p distribution whose peak of negative pressure near the leading edge is much smaller than case 3, and which is distributed flatly from the vicinity of $x/L_{chord}=0.05$ (the region applied the body force) to $x/L_{chord}=1$ (trailing edge). The C_p distribution like this is the typical distribution on the massive separated flow. The flow fields and C_p distributions on the case 1, the case 3 and the case 4 at $\alpha=18$ deg are shown in Fig. 9 and Fig. 10. At this angle of attack, it can be jaded that the massive flow separation is occurred on the case 1. These results indicate that applying the body force near the airfoil surface is effective on the separation control, and the width of the region at which the body force acts in wing surface direction is not very effective to the separation control.



(a) case 1



(b) case 3



(4) case 4

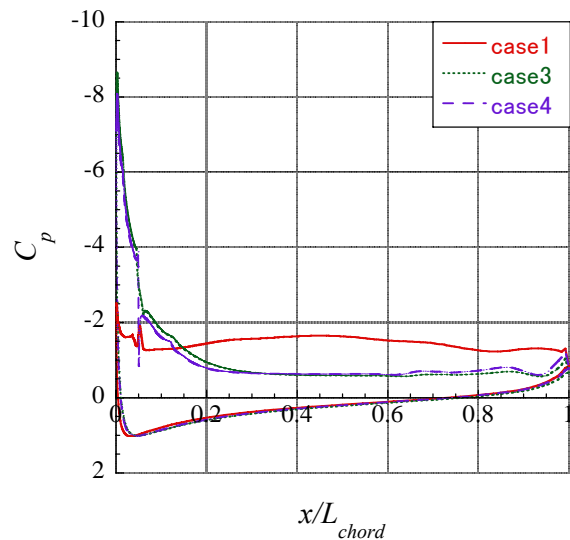
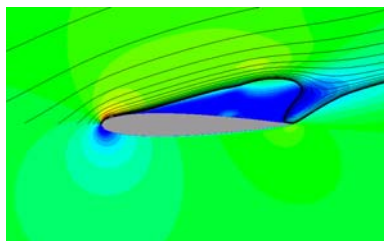


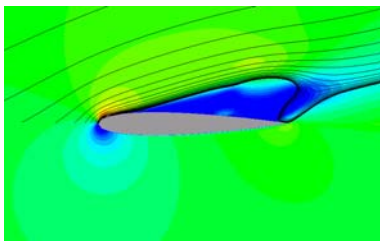
Fig. 9. Flow-fields with stream lines on the case 1, case 2 and the case 4 at $\alpha=19$ deg

Fig. 10. C_p distributions on the case 1, case 2 and the case 4 at $\alpha=19$ deg

Finally, the effect of the body force in the vertical direction to the airfoil surface is discussed. The flow fields and C_p distributions on the Suzen model and the ξ Suzen model at $\alpha=19$ deg are shown in Fig. 11 and Fig. 12. The reason why the C_p value at $x/L_{chord}=0.05$ is partially on Suzen model high is that the induced flow by the body force in the vertical direction to the airfoil surface stagnate, and the pressure increases. As you can see, the flow-fields and the C_p distributions almost same except the C_p value at $x/L_{chord}=0.05$. So, it can be sad that the body force in the vertical direction to the airfoil surface does not so much affect the separation control.



(a) Suzen model



(b) ξ Suzen model

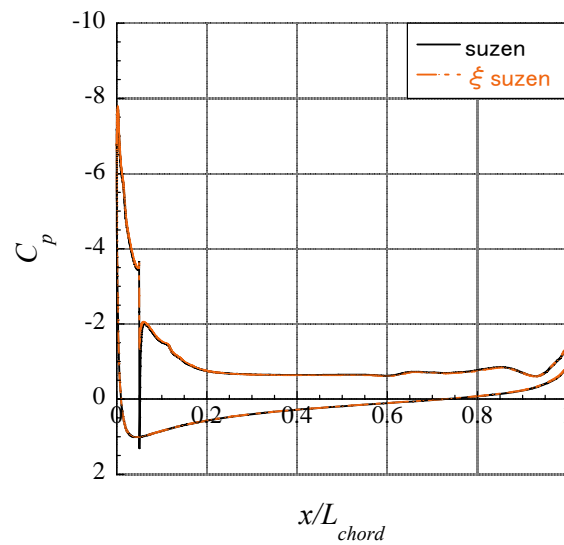
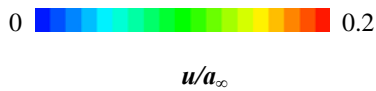


Fig. 11. Flow-fields with stream lines on the Suzen model and the ξ Suzen model at $\alpha=19$ deg

Fig. 12. C_p distributions on the Suzen model and the ξ Suzen model at $\alpha=19$ deg

CONCLUSIONS

Steady body force is applied to the separation flow around the NACA0012 airfoil near the leading edge, and two-dimensional Favre-averaged Navier-Stokes equations are solved by conventional CFD method. The following characteristics are observed from the present results. The model applying the body force near the airfoil surface can restrain the airfoil flow separation than the model applying body force far from the airfoil surface. Therefore, body force near the airfoil surface is effective on the separation control. However, in the direction along the airfoil surface, the width of the region at which the body force acts is not very effective to the separation control. Finally, the body force in the vertical direction to the airfoil surface does not so much affect the separation control.

REFERENCES

- Post, M. L. and Corke, T. C. (2004), "Separation Control on High Angle of Attack Airfoil Using Plasma Actuators," *AIAA J.*, Vol.42 No.11 pp.2177-2184.
- Font, G. and Morgan, W. (2005), "Plasma Discharges in Atmospheric Pressure Oxygen for Boundary Layer Separation Control," *AIAA Paper* 2005-4632.
- Roth, J. R. and Dai, X. (2006), "Optimization of the Aerodynamic Plasma Actuator as an Electrohydrodynamic (EHD) Electrical Device," *AIAA Paper* 2006-1203.
- Tsubakino, D. and Fujii, K. (2007), "Effective Lay-out of plasma Actuators for a Flow Separation Control on a Wing," *AIAA2007-474*.
- Asada, K., Ninomiya, Y., Oyama, A., and Fujii, K. (2009), "Airfoil Flow Experiment on the Duty Cycle of DBD Plasma Actuator," *AIAA Paper* 2009- 531.
- Seifert, A., Darabi, A., Wygnanski, I. (1996), "Delay of Airfoil Stall by Periodic Excitation," *AIAA J. of Aircraft*, Vol.33 No.4 pp.691-698.
- Guynn, M. D., Croom, M. A., Smith, S. C., Parks, R. W., and Gelhausen, P. A. (2003), "Evolution of a Mars Airplane Concept for the ARES Mars Scout Mission," *AIAA Paper* 2003-6578.
- Kawai, S. and Fujii, K. (2005), "Analysis and Prediction of Thin-Airfoil Stall Phenomena with Hybrid Turbulence Methodology," *AIAA Journal*, Vol. 43, No. 5.
- Baldwin, B. and Lomax, H. (1978), "Thin Layer Approximation and Algebraic Model for Separated Turbulent Flows," *AIAA Paper* 1978-257.
- Suzen, Y. B. and Huang, P. G. (2006), "Simulations of Flow Separation Control using Plasma Actuator," *AIAA Paper* 2006-877.
- Shima, E. and Jounouchi, T. (1997), "Role of CFD in Aeronautical Engineering (No. 14) – AUSM Type Upwind Schemes -," 14th NAL Symposium on Air-craft Computational Aerodynamics.
- Liou, M.-S. and Jr, C. J. S. (1991), "A New Flux Splitting Scheme," *Journal of Computational Physics*, Vol. 107.
- Van Leer, B. (1977), "Toward the ultimate Conservative Difference Scheme. IV, A New Approach to Numerical Convection," *Journal of Computational Physics*, Vol. 23, March 1977.
- Fujii, K. (1999), "Efficiency Improvement of Unified Implicit Relaxation/Time Integration Algorithms," *AIAA Journal* , Vol. 37, No. 1, 1999, pp. 125-128.
- Fujii, K. (1986). and Obayashi, S., "Practical Applications of New LU-ADI Scheme for the Three-Dimensional Navier-Stokes Computation of Transonic Viscous Flow," *AIAA Paper* 1986-513.
- Yoon, S. and Jameson, A. (1988), "Lower-Upper Symmetric Gauss-Seidel Method for the Euler and Navier-Stokes Equations," *AIAA Journal*, Vol. 26, No. 9, 1988, pp. 1025-1026.